A&A 407, 551–562 (2003)
DOI: 10.1051/0004-6361:20030881

Astronomy & Astrophysics

^{13}C isotope effects on infrared bands of quenched carbonaceous composite (QCC)

S. Wada[1], T. Onaka[2], I. Yamamura[3], Y. Murata[1], and A. T. Tokunaga[4]

[1] Department of Applied Physics and Chemistry, The University of Electro-Communications, Chofugaoka, Chofu, Tokyo 182-8585, Japan
[2] Department of Astronomy, The University of Tokyo, 7-3-1 Hongo, Bunkyo-ku, Tokyo 113-0033, Japan
[3] The Institute of Space and Astronautical Science (ISAS), Yoshino-dai 3-1-1, Sagamihara, Kanagawa 229-8510, Japan
[4] Institute for Astronomy, University of Hawaii, 2680 Woodlawn Dr., Honolulu, HI 96822, USA

Received 6 May 2003 / Accepted 2 June 2003

Abstract. We investigate carbon isotope effects on the infrared bands of a laboratory analogue of carbonaceous dust, the quenched carbonaceous composite (QCC), synthesized from a plasma gas of methane with various ^{12}C/^{13}C ratios. Peak shifts to longer wavelengths due to the substitution of ^{12}C by ^{13}C are clearly observed in several absorption bands. The shifts are almost linearly proportional to the ^{13}C fraction. New features associated with ^{13}C are not seen, indicating that the infrared bands in the QCC are not very localized vibration modes but come from vibrations associated with rather large carbon structures. An appreciable peak shift ($\Delta\lambda \sim 0.23$–0.26 μm per ^{13}C fraction) is detected in the 6.2 μm band, which is attributed to a carbon-carbon vibration. A peak shift ($\Delta\lambda \sim 0.16$–0.18 μm per ^{13}C fraction) in an out-of-plane bending mode of aromatic C–H at 11.4 μm is also observed, while only a small shift ($\Delta\lambda < 0.015$ μm per ^{13}C fraction) is detected in the 3.3 μm band, which arises from a C–H stretching mode. The present experiment suggests that peak shifts in the unidentified infrared (UIR) bands, particularly in the 6.2 μm band, should be detectable in celestial objects with low ^{12}C/^{13}C ratios (<10). The isotopic shifts seen in the QCC are discussed in relation to the variations in the UIR band peaks observed in post-asymptotic giant branch stars and planetary nebulae. The observed peak shift pattern of the UIR bands is qualitatively in agreement with the isotopic shifts in the QCC except for the 7.7 μm band complex although the observed shifts in the UIR bands are larger than those inferred from derived isotope ratios for individual objects. The poor quantitative agreement may be attributed partly to large uncertainties in the derived ^{12}C/^{13}C, to possible spatial variations of the isotope abundance within the object, and to combinations of other effects, such as hetero-atom substitutions. The present investigation suggests that part of the observed variations in the UIR band peaks may come from the isotopic effects.

Key words. infrared: ISM – dust, extinction – stars: AGB and post-AGB – planetary nebulae: general – ISM: abundances – ISM: lines and bands

1. Introduction

A wide range of the ^{12}C/^{13}C ratio has been reported in various celestial objects. The ratio changes due to nucleosynthesis and mixing in the interior of stars. During the first dredge-up on the red giant branch (RGB) the convective envelope reaches regions abundant in ^{13}C that was processed from ^{12}C and the ratio decreases. Observations of RGB stars often show the ^{12}C/^{13}C ratio of 5–20, even lower than theoretically predicted, suggesting the presence of extra-mixing below the convective envelope (e.g. Gilroy 1989). In the third dredge-up during the asymptotic giant branch (AGB) phase, an increase in ^{12}C/^{13}C is generally expected, but the ratio could also decrease due to cool bottom processing for low-mass stars (Wasserburg et al. 1995; Nollett et al. 2003) or to hot bottom burning for more massive stars (Frost et al. 1998). Observations of five carbon-rich circumstellar envelopes indicate the ratio of 30–65 (Kahane et al. 1992), while ten carbon stars are shown to have the ratio in the range 12–60 in their circumstellar envelopes (Greaves & Holland 1997). Some carbon stars show the ratio of ^{12}C/^{13}C as low as 3 (Lambert et al. 1986; Ohnaka & Tsuji 1996; Schöier & Olofsson 2000). The ^{12}C/^{13}C ratio in post-AGB stars and planetary nebulae (PNe) reflects the cumulative effects of different mixing and nuclear processing events during the entire evolution of their progenitors. Lower limits of the ratio of 3 to 10 have been obtained for several objects in the post-AGB phase (Palla et al. 2000; Greaves & Holland 1997). Recently Josselin & Lébre (2001) estimated an upper limit of ^{12}C/^{13}C of 5 for the post-AGB candidate, HD 179821, whereas a relatively large ratio of 72 ± 26 is reported for another post-AGB star, HD 56126 (Bakker & Lambert 1998). Clegg et al. (1997) found low ratios of 15 and 21 in two PNe. Further low values of the ratio of 2–30

Send offprint requests to: S. Wada,
e-mail: wada@e-one.uec.ac.jp

have been reported in recent studies of several PNe (Palla et al. 2000; Balser et al. 2002; Josselin & Bachiller 2003), suggesting that some stars undergo non-standard processing in the stellar interior and a low $^{12}C/^{13}C$ can be expected during the late stage of their evolution. The solar system value is 89 (Anders & Grevesse 1989).

The $^{12}C/^{13}C$ ratio also provides key information on the chemical evolution in the Galaxy (for a review, Wilson 1999). Observations of molecules and solid CO_2 in interstellar medium indicate that the ratio ranges from 10–100 and increases with the Galactocentric distance. The $^{12}C/^{13}C$ ratio is suggested to be about 10–20 in the Galactic center region (Wilson 1999; Boogert et al. 2000; Savage et al. 2002). The Galactic gradient is thought to be built by nucleosynthesis of the Galactic chemical evolution and the suggested ratio of 10–20 in the Galactic center indicates the presence of significant stellar sources of ^{13}C. Interstellar graphite spherules in the Murchison meteorite show a range of the ratio of 7–1330 (Bernatowicz et al. 1999). Some presolar SiC grains show very low $^{12}C/^{13}C$ ratios of less than 10 and they are thought to originate from very ^{13}C-rich stars in the AGB phase (Amari et al. 2001). These observations suggest that low $^{12}C/^{13}C$ ratio environments are not uncommon in objects in the AGB, post-AGB, and PN phases as well as in some interstellar medium. Carbon-bearing species formed in these environments could thus show non-negligible carbon isotopic effects in their spectrum.

A set of emission bands at 3.3, 6.2, 7.6–7.8, 8.6, and 11.2 μm have been observed in various celestial objects and are called the unidentified infrared (UIR) bands. Fainter companion bands are also sometimes seen. The exact nature of the carriers has not yet been understood completely, but it is generally believed that the emitters or emitting atomic groups containing polycyclic aromatic hydrocarbons (PAH) or PAH-like atomic groups of carbonaceous materials, including such as nanodiamond grains, are responsible for the UIR bands (Léger & Puget 1984; Allamandola et al. 1985; Sakata et al. 1984; Papoular et al. 1989; Arnoult et al. 2000; Jones & d'Hendecourt 2000). Alternatively, Holmid (2000) has recently proposed de-excitation of Rydberg matters as possible carriers. The UIR bands have been observed in a wide range of objects, including H II regions, reflection nebulae, post-AGB stars, and PNe (for a review, see Tokunaga 1997). They have also been commonly seen in the diffuse Galactic emission (Tanaka et al. 1996; Onaka et al. 1996; Mattila et al. 1996; Kahanpää et al. 2003) as well as in external galaxies (e.g. Mattila et al. 1999; Helou et al. 2000; Reach et al. 2000; Lu et al. 2003), indicating that the carriers are a common member of interstellar medium and present in various environments. Carbon-rich objects in the evolutionary stage from post-AGBs to PNe often show the emission bands and thus isotopic effects should be detectable if they arise from carbonaceous materials of low $^{12}C/^{13}C$ ratios. Simple calculations of a ^{13}C-benzene molecule suggest that the peak shift can be as much as 0.15 μm for the C−C stretching mode (Appendix A).

Observations of the Infrared Space Observatory (ISO; Kessler et al. 1996) have provided a large database of the UIR band spectra in various objects (e.g. Beintema et al. 1996; Molster et al. 1996; Verstraete et al. 1996, 2001; Boulanger 1998; Cesarsky et al. 2000a,b; Uchida et al. 1998, 2000; Moutou et al. 2000; Honey et al. 2001). Recently Peeters et al. (2002) have investigated in detail the 6–9 μm spectra of 57 sources taken by the Short Wavelength Spectrometer (SWS; de Graauw et al. 1996) on board the ISO and found that the 6.2, 7.7, and 8.6 μm UIR bands show appreciable variations particularly for post-AGB stars and PNe. On the other hand, the variations in the 11.2 μm band are relatively modest and those in the 3.3 μm are less pronounced (Tokunaga et al. 1991; Roche et al. 1991; Hony et al. 2001; van Diedenhoven et al. 2003). These variations can be interpreted in part by nitrogen substitutions in PAHs and anharmonicity, but not all of the observed aspects of the UIR bands have yet been fully understood (Verstraete et al. 2001; Pech et al. 2002; Peeters et al. 2002). Part of the observed variations could also originate from isotopic effects of the UIR band carriers since the objects that show the variations are mostly post-AGB stars and PNe, in which small $^{12}C/^{13}C$ ratios can be expected.

In the present paper we investigate isotopic effects on the UIR bands experimentally. We synthesize a laboratory analogue of carbonaceous dust, the quenched carbonaceous composite (QCC; Sakata et al. 1984), with various $^{12}C/^{13}C$ ratios from the starting gas of a mixture of $^{12}CH_4$ and $^{13}CH_4$. The QCC shows infrared bands similar to the UIR bands and shifts in the band peaks due to the ^{13}C substitution are clearly detected. In Sect. 2 we describe the experimental procedure. The results are shown in Sect. 3 and discussed in comparison with observations in Sect. 4. A summary is given in Sect. 5.

2. Experimental

The experimental procedure for synthesizing the QCC is described in detail in Sakata et al. (1984). Methane (CH_4), the source gas of the QCC, is decomposed by the imposed microwave radiation and becomes a plasma. Carbonaceous condensates are formed in the injection beam of the plasma by quenching of the gas. Typically two types of the QCC are formed. One is a brown-black material (hereafter called dark-CC), which is collected on a substrate in the main injection beam. It has been shown to consist of a coagulation of carbon-onion-like particles (Wada et al. 1999). The other is a yellow-brownish material (hereafter filmy-QCC), deposited on the surrounding region of the injected plasma gas (Sakata et al. 1987). It is a material rich in organic molecules, such as PAHs. We prepare the starting gas of CH_4 with the ^{13}C fraction of 1%, 11%, 25%, 45%, 65% and 99% by mixing 99% ^{13}C methane with the natural isotope abundance (1% ^{13}C) methane. We assume that the ^{13}C fraction in the QCC is equal to that of the starting gas in the present analysis because the reactions in the present experiments take place at high temperatures.

The QCC is collected either on a KBr (for filmy-QCC) or on a BaF_2 crystal (for dark-QCC) and the absorption spectra are measured at room temperature. The spectra are taken by a Perkin-Elmer 2000-FTIR spectrometer with the resolution of 4 cm^{-1}. The spectra of the dark-QCC are measured after washing it with a small amount of acetone and removing organic molecules in the dark-QCC in a similar manner to previous experiments (Sakata et al. 1984).

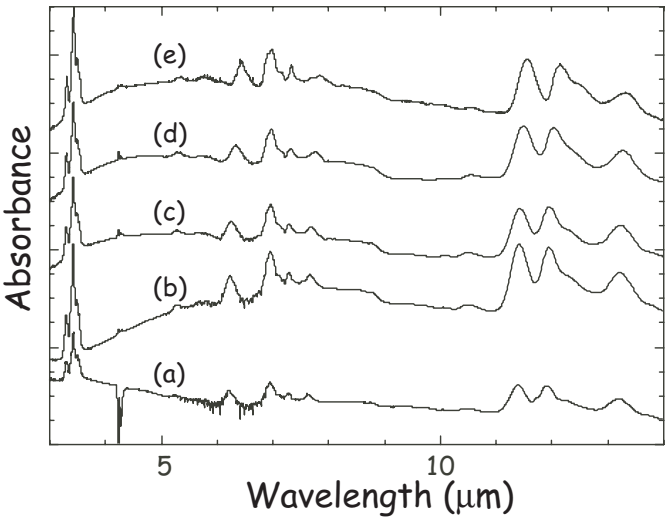

Fig. 1. Absorption spectra of filmy-QCC with various ^{13}C fractions. The ^{13}C fractions are **a)** 1%, **b)** 11%, **c)** 25%, **d)** 65%, and **e)** 99%. Each curve is shifted arbitrarily in the vertical direction.

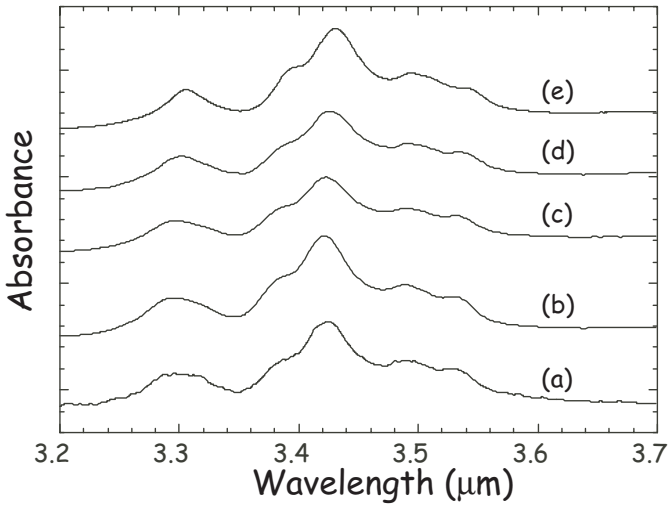

Fig. 2. Spectra of the filmy-QCC in the 3 μm region. The ^{13}C fractions are **a)** 1%, **b)** 11%, **c)** 25%, **d)** 65%, and **e)** 99%. Each curve is shifted arbitrarily in the vertical direction.

3. Results

The isotopic substitution gives rise to a shift in the wavelength of vibration modes due to mass effects. With the replacement of ^{12}C with ^{13}C, the infrared band is expected to be shifted to longer wavelengths.

3.1. Spectra of filmy-QCC

The filmy-QCC is a coagulation of many kinds of organic molecules. Mass analysis of the gases evaporating from the filmy-QCC shows that they contain various kinds of PAHs. The filmy-QCC also emits red fluorescence under ultraviolet irradiation (Sakata et al. 1992).

The spectra of the filmy-QCC with various ^{13}C fractions are shown in Fig. 1. They show several absorption features similar to the UIR bands observed in celestial objects (Sakata et al. 1984, 1987, 1990). For the filmy-QCC with 1% ^{13}C the bands of the C−H stretching characteristic group appear at 3.29, 3.42, 3.51, and 3.53 μm (see also Fig. 2). An aromatic C=C bond vibration appears at 6.2 μm, and aromatic C−H out-of-plane bending modes are observed at 11.4, 11.9, and 13.2 μm. A weak feature also appears clearly at 7.6 μm in addition to the bands at 7.0 and 7.3 μm. A very broad band is seen around 8.6 μm, but its peak wavelength cannot be determined accurately because of the weak and broad feature. All the features observed in the samples of various ^{13}C fractions have corresponding features in the 1% ^{13}C sample and the peak wavelengths are shifted to longer wavelengths with the ^{13}C fraction. No new absorption band associated with ^{13}C appears.

A large shift ($\Delta\lambda \sim 0.23\,\mu$m between 1% to 99% ^{13}C) is observed in the 6.2 μm band. The C−C mode involves at least two carbon atoms and makes the shift large. The shifts in the peaks arising from C−H out-of-plane bending modes are also seen. The 11.39 μm peak at 1% ^{13}C shifts to 11.55 μm at 99% ^{13}C. On the other hand, the shift in the 3.29 μm band of aromatic C−H stretching is quite small ($\Delta\lambda \sim 0.014\,\mu$m). Figure 2 shows the spectra expanded in the 3 μm region. It is noticeable that the profile of the 3.3 μm band becomes narrower with the ^{13}C fraction. The cause of this change is unknown at present. A small shift is also observed in the 3.4 μm band, which is attributed to an asymmetric vibration of methylene (C−H_2).

The peak wavelength of the small feature at 7.6 μm is also shifted to longer wavelengths with the ^{13}C fraction ($\Delta\lambda \sim 0.22\,\mu$m). The large shift indicates that the vibration involves more than one carbon atoms, such as C−C. The broad bump at 8.6 μm does not shift clearly. Sakata et al. (1987) assigned the 7.6 and 8.6 μm peaks of the filmy-QCC to vibration modes of a kind of the ketone bond C=C−C=O. The 7.6 μm peak is always observed in the filmy-QCC spectrum although the relative strength changes slightly with individual runs. The exposure to air does not increase the strength of the 7.6 μm band. The present experiment thus suggests that the 7.6 μm component is a molecular product of the plasma gas and is not directly related to oxidation.

3.2. Spectra of dark-QCC

High-resolution electron-microscopy reveals that the dark-QCC is comprised of a coagulation of onion-like particles of the diameter of 10–15 nm (Wada et al. 1999). It is insoluble in acetone. Even after washing with acetone, the dark-QCC still contains some organic molecules. Mass spectroscopy indicates that they are mainly composed of compact PAHs. The dark-QCC adsorbs organic molecules that are formed together and also contains hydrogen atoms in its structure. C−H bonds in both components will give rise to vibration modes in the infrared. Figure 3 shows the absorption spectra of the dark-QCC with 1% ^{13}C fraction together with the filmy-QCC spectrum for comparison. The dark-QCC shows a strong continuum component, which decreases with the wavelength. Small peaks are observed at 3.3, 3.42, 5.8, 6.3, 7.0, 7.3, 8.2, 11.4, 12.0, and 13.2 μm. The 3.3, 3.42, 11.4, 12.0, and 13.2 μm bands are attributed to CH vibrations, and the

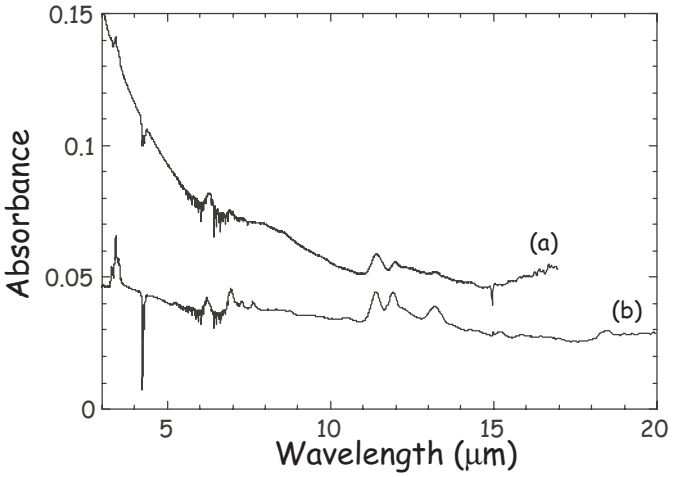

Fig. 3. Absorption spectra of **a)** dark-QCC and **b)** filmy-QCC with the natural isotopic fraction (^{13}C = 1.1%).

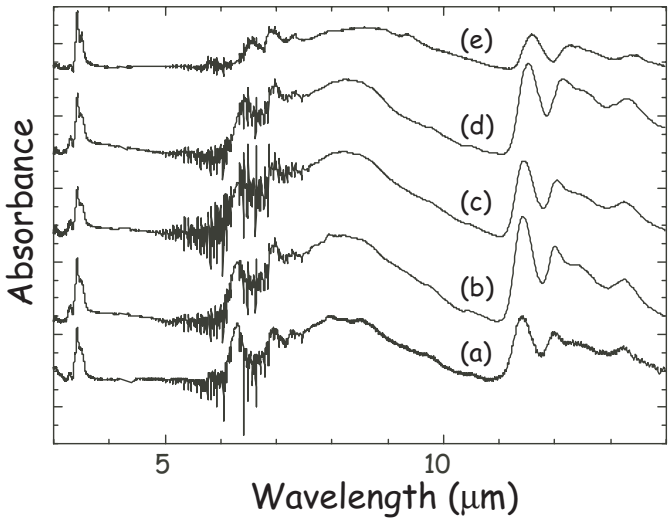

Fig. 4. Absorption spectra of the dark-QCC with various ^{13}C fractions with the continuum subtracted. The ^{13}C fractions are 1% **a)**, 11% **b)**, 25% **c)**, 65% **d)**, and 99% **e)**. Each curve is shifted arbitrarily in the vertical direction.

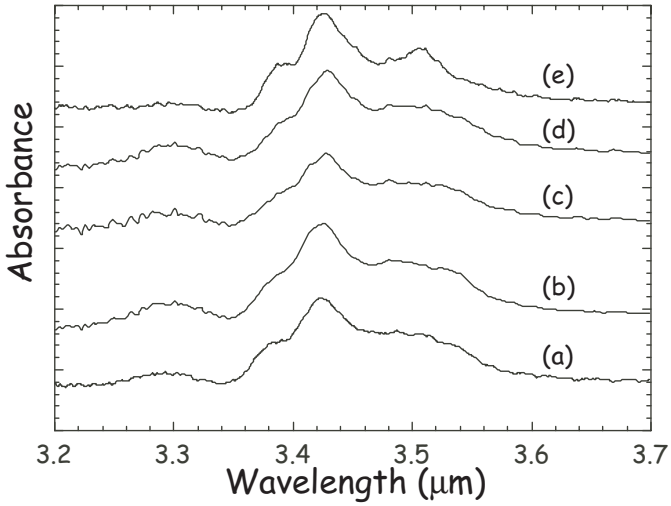

Fig. 5. Spectra of the dark-QCC in the 3 μm region. The ^{13}C fractions are **a)** 1%, **b)** 11%, **c)** 25%, **d)** 65%, and **e)** 99%. Each curve is shifted arbitrarily in the vertical direction.

6.3 μm band is ascribed to an aromatic C=C bond vibration. The broad 8.2 μm band becomes strong when it is exposed to air. An increase of the 5.8 μm band is also seen during the exposure to air, suggesting that both of them are associated with C−O− and C=O bonds formed by oxidation.

Figure 4 shows the absorption spectra of the dark-QCC with various ^{13}C fractions. The continua were fitted with cubic spline functions and have been subtracted to show the absorption features clearly. As in the filmy-QCC spectra, peak shifts with the ^{13}C fraction are clearly observed and new features without corresponding ones in the 1% ^{13}C sample are not seen in large ^{13}C fraction samples. A large shift ($\Delta\lambda \sim 0.26$ μm) is again observed for the 6.3 μm band. The peak position of the 8.2 μm band cannot be measured accurately because of the wide profile, but the peak is clearly shifted to longer wavelengths with the ^{13}C fraction. The band width also seems to change. Particularly for the 99% ^{13}C sample the 8.2 μm feature becomes very broad. The 3.3 μm band is quite weak in the dark-QCC and the peak position of the 3.3 μm is difficult to determine (see Fig. 5). The feature almost fades away in the 99% ^{13}C sample. The change in the profile of the 3.3 μm seen in the filmy-QCC sample is not observed in the dark-QCC.

3.3. Peak shifts of the absorption bands

Figure 6 plots the peak wavelength of each band against the ^{13}C fraction. The change of the peak wavelength is roughly linear with the ^{13}C fraction for all the bands plotted. Linear lines obtained by least-squares fits are also shown. The slope of the fitted line is given in Table 1 together with the shifts estimated from the calculation of ^{12}C- and ^{13}C-benzene (Appendix A). The amount of the shift in the 6.2 μm band is large and even larger than the estimate based on the simple calculation of benzene molecules. The shift of the 11.4 μm band is also larger than the calculation. The shift in the 3.3 μm band of the filmy-QCC is in agreement with the calculation, while that of the dark-QCC is smaller than the calculation. It should be noted, however, that the 3.3 μm band of dark-QCC is weak and the peak position cannot be determined accurately (Fig. 5).

The present experiment shows no new features corresponding to ^{13}C. If the vibration mode is local, there should appear peaks corresponding to ^{12}C and ^{13}C. The spectral resolution is sufficiently high except for the 3.3 μm band, which shows only small shifts, but any appreciable broadening of the feature that indicates a combination of multiple peaks is not seen with the ^{13}C fraction. Thus the peak shift cannot be interpreted in terms of a combination of the components corresponding to ^{12}C and ^{13}C. The present results indicate that the vibration modes in the QCC are not very localized, but involve rather large molecular structures. The peak shift is related to the number of carbon atoms involved in the vibration mode. The larger shift than the calculation suggests that more than two carbon atoms are associated with the 6.2 μm band of the QCC. The large shift in the 11.4 μm band also indicates that this feature

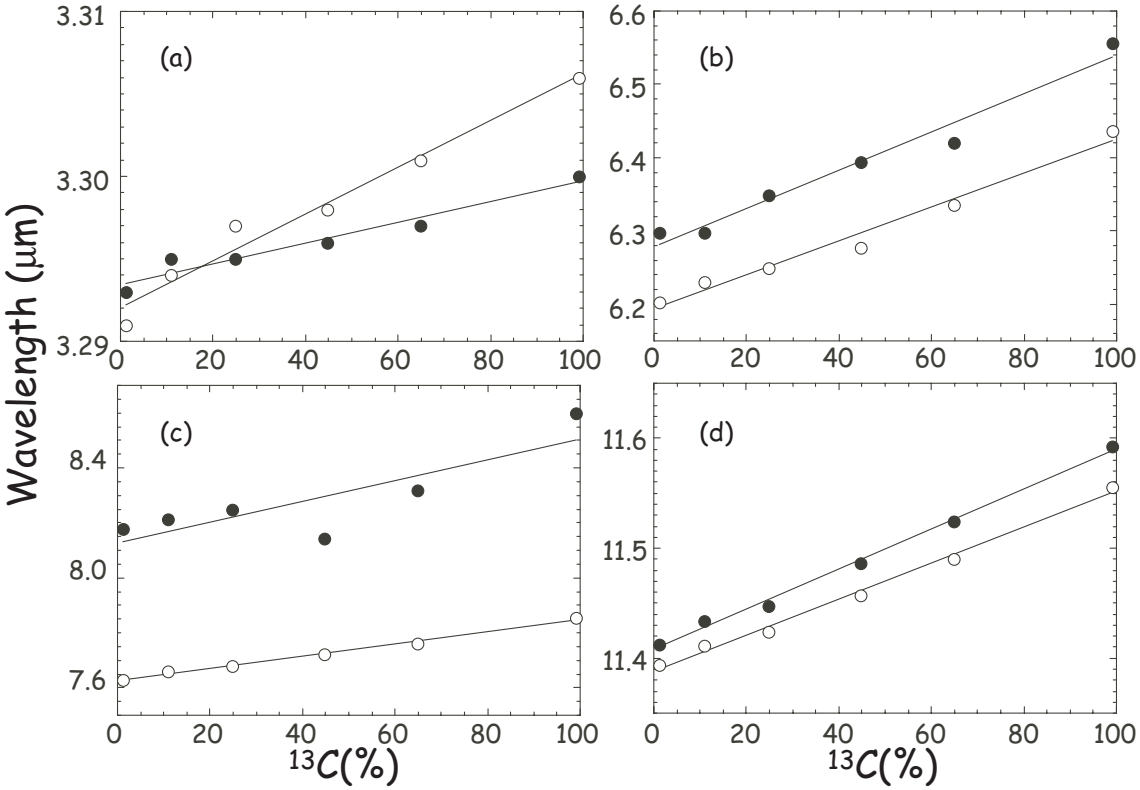

Fig. 6. Peak wavelength versus ^{13}C fraction of the filmy-QCC (open circles) and the dark-QCC (filled circles). **a)** Aromatic C−H stretching modes, **b)** aromatic C=C vibration modes, **c)** 7.6 and 8.2 μm bands, and **d)** C−H out-of-plane bending modes. Least-squares fit lines are also plotted.

Table 1. Peak shift of the absorption bands in the QCC and the UIR bands.

Peak wavelength of ^{12}C QCC (μm)	Slope of the fitted line (μm per ^{13}C fraction)		Estimated shift between ^{12}C and ^{13}C benzene[a] (μm)	Observed range of the peak wavelength[b] (μm)
	filmy-QCC	dark-QCC		
3.3	0.014 ± 0.001	0.0063 ± 0.0007[c]	0.013	3.288–3.297
6.2	0.231 ± 0.018	0.262 ± 0.023	0.14	6.20–6.27 (6.30)
7.6	0.219 ± 0.010	–	–	7.72–7.97[d]
8.2	–	0.379 ± 0.124[c]	–	(~8.22)
11.4	0.163 ± 0.007	0.183 ± 0.007	0.04	11.20–11.25

[a] See Appendix A.
[b] The observed range between class *A* and *B* objects taken from Tokunaga et al. (1991), Peeters et al. (2002), and van Diedenhoven et al. (2003). The peak wavelengths of class *C* objects are indicated in parentheses (see text).
[c] The slopes have large uncertainties because of the broad feature.
[d] The peak wavelength range of the 7.8 μm subcomponent (see text).

originates from CH bonds associated with large benzene structures if it is ascribed to a CH out-of-plane bending mode.

The two kinds of the QCC have very different chemical compositions from each other. The spectrum of the dark-QCC shows a continuum component, which indicates the development of sp^2 carbon-carbon bonds. The broad bump around 8.2 μm and the strong continuum are the characteristics of carbon-rich particles. The filmy- and dark-QCC have absorption bands at similar wavelengths, but the bands seen in the dark-QCC always peak at longer wavelengths than the filmy-QCC except for the 3.3 μm band with large ^{13}C fractions (Fig. 6). The isotopic shift appears similar both in the filmy-QCC and dark-QCC except for the 3.3 μm band. The 3.3 μm band in the dark-QCC is rather weak and thus further examination is needed to understand the different behavior of the 3.3 μm band between the filmy- and dark-QCC.

4. Discussion

The infrared spectra of the QCC show several similarities to the observed UIR bands, but they are not exactly the same. The peak wavelength of the 3.3 μm band of the f-QCC is in

agreement with observations (Sakata et al. 1990), while the exact peak wavelengths are not at the right positions for some other bands and there are differences in the band profiles. The 11.4 μm band in the QCCs is obviously located at a longer wavelength than observed (11.23–11.25 μm). Some UIR bands, such as the 6.2 μm and 11.2 μm bands, are not symmetric, but skewed to longer wavelengths, whereas most bands in the QCC seem to be more or less symmetric. Therefore a direct comparison of the QCC spectra with observations is not very straightforward since the QCC is probably not the very material that exists in interstellar space. However we believe that the QCC contains many of the structural units corresponding to the material in the interstellar medium because of the spectral similarities of the QCC and the UIR bands. In the following we examine whether or not observed variations of the UIR bands seen in post-AGB stars and PNe can be accounted for by the isotopic shifts observed in the QCC. We concentrate on the relative shifts in the band peaks of the QCC and the absolute peak wavelengths and band profiles are not discussed. The results of the filmy-QCC are compared with the observations for clarity because the difference in the relative shifts between filmy- and dark-QCC is small except for the 3.3 μm band.

Peeters et al. (2002) have investigated the 6–9 μm UIR bands in various objects and found that there are at least three classes, designated as *A*, *B*, and *C*, according to the peak wavelengths of the emission bands. Class *A* is a major class and includes a wide range of objects, such as H II regions, non-isolated young stellar objects (YSOs), reflection nebulae, and galaxies. They do not show appreciable variations in the 6.2, 7.7, and 8.6 μm band features. Class *B* consists of isolated YSOs, post-AGB stars, and PNe. They exhibit quite a large variation in the peak wavelengths of the 6–9 μm features. The peaks are all shifted to longer wavelengths compared to class *A* objects. The observed ranges of the peak wavelengths are listed in Table 1. The apparent variation in the 7.7 μm complex comes partly from the change in the relative strengths of the subcomponents. The peak shift in the 7.8 μm subcomponent is well observed, while that in the 7.6 μm subcomponent is less clear. Table 1 indicates the observed range of the peak wavelength of the 7.8 μm subcomponent. Class *C* consists of only two objects (CRL 2688 and IRAS 13146−6243). They show a very different spectrum from the other two classes. They have a band at 6.3 μm but do not show any features around 7.7 and 8.6 μm. Instead they show a broad band at 8.22 μm. Hence class *C* objects seem to have different kinds of the band carriers from those in classes *A* and *B*. In the following discussion the peak wavelength of the 6.3 μm band in class *C* objects is not included in the observed variation since it will probably not be directly related to the isotopic effects. Although there are some internal variations present, the class in the 6–9 μm bands is well defined and almost all class *B* objects show the peaks shifted to longer wavelengths in all the 6.2, 7.7, and 8.6 μm bands.

Compared to the 6–9 μm spectrum, the 3.3 and 11.2 μm UIR bands show small variations (Hony et al. 2001), but the variations in the peak position do exist (e.g. Nagata et al. 1988; Tokunaga et al. 1988; Roche et al. 1991). Tokunaga et al. (1991) have suggested that there are two types of the 3.3 μm band from a small number of objects. Type 1 is a major class, in which the peak is located at 3.289 μm, while type 2 has the peak at 3.296 μm. They also suggest that type 2 objects have a narrower width than type 1. van Diedenhoven et al. (2003) have extended the investigation of the 3.3 and 11.2 μm UIR bands on the same sample as in Peeters et al. (2002). They found that there are also two classes in each band, designated as $A_{3.3}$, $B_{3.3}$, $A_{11.2}$, and $B_{11.2}$, respectively. Class $A_{3.3}$ corresponds to type 1 and $B_{3.3}$ to type 2 in Tokunaga et al. (1991). $A_{3.3}$ and $A_{11.2}$ are major classes, and $B_{3.3}$ and $B_{11.2}$ classes show the bands at 3.3 μm and 11.2 μm shifted to longer wavelengths compared to $A_{3.3}$ and $A_{11.2}$, respectively. The observed ranges of the shifts in the 3.3 and 11.2 μm bands are also shown in Table 1. The shift in the 3.3 μm band is quite small and that in the 11.2 μm band is modest. In general objects classified as class *B* in the 6–9 μm spectrum are also classified as $B_{3.3}$ and $B_{11.2}$, but the correlation is not very good. Objects classified as class *B* in the 6–9 μm spectrum sometimes do not show detectable shifts in the 3.3 and 11.2 μm bands (e.g. BD +30 3639) and vice versa (e.g. He2−113). van Diedenhoven et al. (2003) concluded that the appearance of the 3.3 and 11.2 μm band variations is not tightly correlated with the UIR bands in 6–9 μm.

The present results suggest that if $^{12}C/^{13}C < 10$ the isotopic shifts are detectable particularly in the 6.2 and 7.7 μm bands. A low $^{12}C/^{13}C$ ratio of this range is often suggested in post-AGB stars and PNe, and thus part of the peak shifts in these objects could be attributed to the isotopic effects. The shift in the 11.2 μm of a medium degree can also be expected, while the shift in the 3.3 μm should be small. This shift pattern is qualitatively compatible with observations except for the 7.8 μm band. The 7.8 μm subcomponent shows a larger shift in its peak wavelength compared to the QCC sample. The 7.7 μm complex exhibit complicated profile variations and there may be other weak subcomponents present. The observed range of the 3.3 μm, 6.2 μm, and 11.2 μm bands suggest that the objects with the largest shifts should have $^{12}C/^{13}C \sim 2$.

We have searched in literature for the $^{12}C/^{13}C$ ratio of objects that had been observed by ISO/SWS. Table 2 lists the objects and the SWS observing modes. SWS01 was the full grating scan mode and the spectral resolution depends on the scan speed. SWS06 was the fixed-range grating scan mode and provided the highest spectral resolution in the grating mode of SWS (Leech et al. 2002). We used the highest spectral resolution data as much as possible if there are several observations made for the same object. IRAS 23133+6050 is included in the list as a reference of the class *A* object. The Off-Line Processing data of version 10.1 (OLP 10.1) were obtained from the ISO Archival Data Center and reduced further by the Observers SWS Interactive Analysis Package (OSIA) version 3.0[1]. The peak wavelength for each band is estimated after the local continuum has been subtracted (see Fig. 7). The peak position is slightly dependent on the assumed local continuum. Strong Pfδ (3.29699 μm) has been removed in the estimation of the peak wavelength of the 3.3 μm band for IRAS 23133+6050,

[1] The OSIA is a joint development of the SWS consortium. Contributing institutes are SRON, MPE, KUL and the ESA Astrophysics Division.

Table 2. Objects and the ISO/SWS observation mode.

Name	Type	TDT[a]	Obs. mode[b]
IRAS 23133+6050[c]	H II region	56 801 906	SWS01 (2)
IRAS 21282+5050	post-AGB	15 901 777	SWS01 (3)
NGC 7027	PN	33 800 505	SWS06
BD +30 3639	PN	86 500 540	SWS01 (3)
IC 5117	PN	36 701 824	SWS01 (1)
HR 4049	post-AGB	17 100 101	SWS01 (2)
HD 44179	post-AGB	70 201 801	SWS01 (4)
CRL 2688	post-AGB	33 800 604	SWS06

[a] Target Dedicated Time (TDT) of the ISO observation.
[b] Number in brackets indicates the scanning speed of the SWS01 mode.
[c] Reference object of class *A*.

NGC 7027, and BD +30 3639. Table 3 lists the objects with the derived isotope ratio and their observed peak wavelengths. The peak wavelengths are in agreement with previous investigations within the uncertainty (Nagata et al. 1988; Tokunaga et al. 1991; Peeters et al. 2002). The objects are listed in the order of the peak wavelength of the 6.2 μm band. Each band spectrum is normalized at the peak after the continuum has been subtracted and shown in Fig. 7.

Very few data of the carbon isotope abundance are available for post-AGB stars. Observations of ^{13}C isotopic lines of C_2, CN, and CH^+ in several post-AGB stars resulted in negative detection of molecular features of ^{13}C except for one object (Bakker et al. 1997, 1998). They thus provided only lower limits for the ^{12}C/^{13}C ratio of >10−20. The carbon isotope ratios in a few post-AGB stars and several PNe have been obtained mostly from radio observations of CO molecules. The intensity ratio of ^{12}CO to ^{13}CO emission is thought to be a good measure for the isotope ratio if both lines are optically thin since the selective photodissociation of ^{13}CO should be counterbalanced by the charge exchange reaction (e.g. Mamon et al. 1988). However ^{12}CO lines often become optically thick, only lower limits of ^{12}C/^{13}C being estimated. It should also be noted that observations of CO probe the entire region of the circumstellar envelope. The post-AGB is a transient phase and a rapid change of the abundance is expected to occur in their envelopes. Thus the isotope ratio in the vicinity of the star might be different from that inferred from the CO intensity ratio.

IRAS 21282+5050 is a post-AGB star and classified as class *A* in the 6–9 μm spectrum and $A_{3.3}$. The 3.3 μm band peaks around 3.288–3.290 μm (e.g. Nagata et al. 1988). Likkel et al. (1988) obtained that the intensity ratio of ^{12}CO/^{13}CO (J = 1−0) is about 100 and inferred ^{12}C/^{13}O ∼ 200, taking account of the optical thickness effect of ^{12}CO. Based on the large gradient velocity model analysis, Balser et al. (2002) obtained ^{12}C/^{13}C > 32 from observations of CO J = 2−1 and J = 3−2 transitions. The observed peak wavelengths are compatible with the large ^{12}C/^{13}C ratio.

NGC 7027 is a bright young PN. It shows the class *A* 6.2 μm band feature, while the 7.7 and 11.2 μm bands are slightly shifted to longer wavelengths relative to class *A*. Also the 7.8 μm component is stronger than the 7.6 μm component, indicating a signature of the class *B* object. The 3.3 μm band peak appears at the normal (class *A*) wavelength. This object has been observed by several groups in ^{13}CO molecular lines. Because of the optical depth effect of ^{12}CO the CO line intensity ratio should be taken as lower limits for the isotope abundance ratio of ^{12}C/^{13}C. They range from 65 (CO(J = 1−0); Kahane et al. 1992) to a recent value of 11 (CO(J = 2−1); Josselin & Bachiller 2003), suggesting that the ^{12}C/^{13}C ratio in the CO envelope of NGC 7027 is probably not less than 10. Except for the 7.7 μm band appearance the suggested range of ^{12}C/^{13}C is compatible with the class *A* classification.

BD +30 3639 is a young PN and classified as class *B* in the 6–9 μm spectrum. Palla et al. (2000) reported a tentative detection of ^{13}CO (J = 2−1) and obtain a lower limit of ^{12}C/^{13}C as ≥4. This object shows medium size band shifts, which can be accounted for by the isotopic shifts with ^{12}C/^{13}C ∼ 5. The corresponding shift in the 3.3 μm would be only ∼0.03 μm, which is also compatible with the observed peak position. The 11.2 μm band shows a large tail in the longer wavelength side.

Assuming that CO lines are optically thin, Palla et al. (2000) derived the ^{12}C/^{13}C of 14 for IC 5117, while Josselin & Bachiller (2003) indicated the ratio of 23 in this object. IC 5117 was not included in the sample of Peeters et al. (2002). The SWS spectrum is noisy and the peak wavelengths cannot be determined accurately. However it clearly indicates the characteristics of the class *B* spectrum. The 7.7 μm band complex is dominated by the 7.8 μm component and the 3.3 and 6.2 μm bands peak at longer wavelengths than class *A*. The indicated ^{12}C/^{13}C ratio seems to be too small to account for the observed spectrum by the isotopic effects, although a qualitative comparison is difficult because of large uncertainties in the peak wavelengths.

HR 4049 is a very metal-poor post-AGB star and it is difficult to estimate its carbon isotope ratio because of very few metallic lines detected in its spectrum. Recently Cami & Yamamura (2001) have investigated circumstellar CO_2 features in the infrared region and suggested that this star has a very peculiar oxygen isotope ratio, such that ^{17}O and ^{18}O are quite enhanced. They have detected $^{13}C^{16}O_2$, $^{16}O^{13}C^{18}O$, and $^{16}O^{13}C^{17}C$ lines, and the intensity ratios of the ^{13}C to ^{12}C lines were all about 0.6–0.7. Although detailed analysis is required to derive a reliable ratio, this implies that HR 4049 is quite rich also in ^{13}C. The positive correlation of ^{12}C/^{13}C with ^{16}O/^{17}O seen in several environments (Wannier & Sahai 1987) also suggests a low ^{12}C/^{13}C ratio. CO_2 molecular emission originates from the region near the star and thus the derived ratio should correspond to the region in which the UIR bands are also emitted. The observed UIR bands in HR 4049 are all shifted to longer wavelengths relative to normal class *A* positions, which can be accounted for by isotopic shifts with ^{12}C/^{13}C ∼ 3. The small ^{12}C/^{13}C ratio suggested by the CO_2 line emissions is compatible with the observed shifts.

HD 44179 is a well-studied post-AGB star and very bright in the infrared. Greaves & Holland (1997) made observations of CO (J = 2−1) and obtained the peak intensity ratio of 2.2 ± 0.2 for ^{12}CO/^{13}CO. The central part of the ^{12}CO

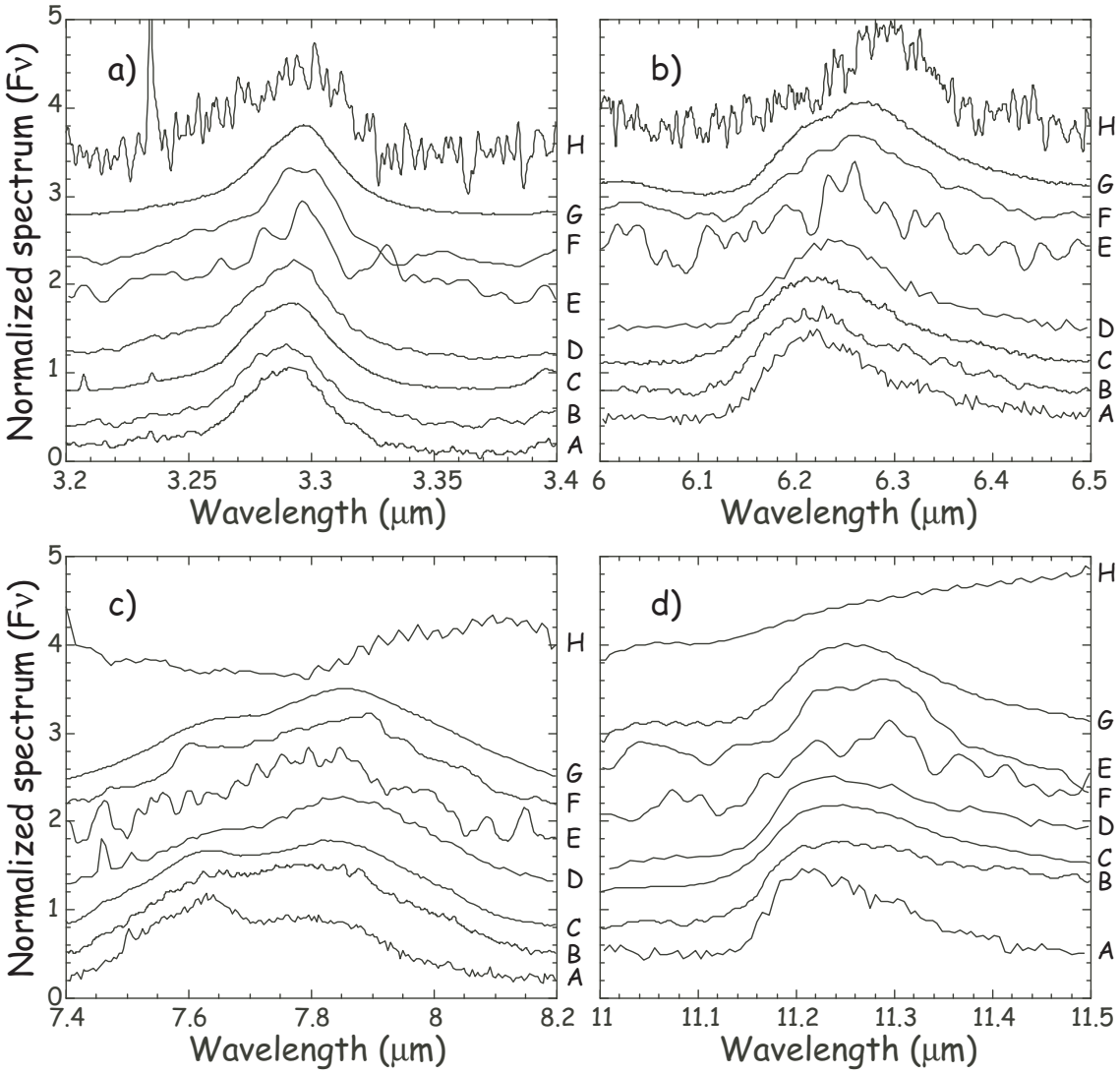

Fig. 7. UIR band spectra of the objects with the measured $^{12}C/^{13}C$ ratio. **a)** the 3.3 μm band, **b)** 6.2 μm band, **c)** 7.8 μm band, and **d)** 11.2 μm band. A: IRAS 23133+6050, B: IRAS 21282+5050, C: NGC 7027, D: BD +30 3639, E: IC 5117, F: HR 4049, G: HD 44179, and H: CRL 2688. The spectra are normalized after the local continua have been subtracted. Strong line emissions have been removed for clarity.

profile appears optically thick and from the wing of the profile they estimate $^{12}CO/^{13}CO \geq 12.5$. The negative detection of $^{13}CH^+$ suggests $^{12}C/^{13}C \geq 22$ (Bakker et al. 1997). The 6–9 μm spectrum of HD 44179 belongs to class *B* and shows one of the largest shifts in the peak wavelengths among the class. HD 44179 is also the only one object that shows two subcomponents in the 6.2 μm clearly. The 3.3 μm band of HD 44179 is of type 2 and peaks at 3.296 μm. The 11.2 μm band is also shifted to 11.25 μm. These shifts can be accounted for consistently by the isotopic effects if $^{12}C/^{13}C$ is ∼2. This required ratio is obviously smaller than the one indicated by CO and $^{13}CH^+$ observations. A complicated torus-bipolar cone structure resulted from a transition from oxygen-rich to carbon-rich envelope has been suggested in HD 44179 (Waters et al. 1998; Men'shchikov et al. 2002), indicating that the carbon isotope ratio may also spatially vary. In fact Kerr et al. (1999) have indicated that the 3.3 μm band peak changes with positions within the nebula and that the longer wavelength peak appears near the star and the interface region of the biconical structure. The ^{13}CO emission with a similar strength to ^{12}CO has also been detected for the 4.6 μm bands in the nebular region (Waters et al. 1998). Two components seen in the 6.2 μm band in HD 44179 may then be ascribed to the band carriers with a small ^{13}C isotope abundance in the outer part and to those with a low $^{12}C/^{13}C$ formed in the region close to the star. Unless there is an appreciable increase in the ^{13}C abundance in the vicinity of the star, however, the observed peak shifts in HD 44179 cannot be accounted for by isotopic effects alone. High-spatial resolution observations in other UIR bands are interesting to investigate possible spatial variations in their peaks (Song et al. 2003).

CRL 2688 is a carbon-rich post-AGB star which shows a peculiar 6–9 μm spectrum (class *C*). The integrated intensity ratio of ^{12}CO to ^{13}CO ($J = 2-1$) is about 3–4 (Wannier & Sahai 1987; Bachiller et al. 1997). The ^{12}CO line is optically thick and thus this gives a lower limit. Wannier & Sahai (1987)

Table 3. Peak wavelengths and carbon isotope ratios of the objects observed with ISO/SWS.

Object	Peak wavelength (μm)				$^{12}C/^{13}C$	Reference[b]
	3.3 μm	6.2 μm	7.8 μm	11.2 μm		
IRAS 23133+6050	3.289	6.219	7.795	11.218		
IRAS 21282+5050	3.290	6.219	7.817	11.245	>200, >32	1, 2
NGC 7027	3.292	6.222	7.830	11.247	>31, >65, >25, >11	3, 4, 5, 6
BD +30 3639	3.292	6.240	7.850	11.237	≥4	7
IC 5117	3.295:	6.25:	7.82:	11.28:	23, 14	6, 7
HR 4049	3.296:[c]	6.256	7.880:	11.285	~1.5[a]	8
HD 44179	3.296	6.267	7.861	11.250	≥22, ≥12.5	3, 9
CRL 2688	3.297	6.290	–	–	>19, 32^{+10}_{-7}, >3, 20^{+8}_{-6}, 5	3, 4, 5, 10, 11

[a] Intensity ratio of CO_2 bands (Cami & Yamamura 2001).
[b] References: 1: Likkel et al. (1988); 2: Balser et al. (2002); 3: Bakker et al. (1997); 4: Kahane et al. (1992); 5: Bachiller et al. (1997); 6: Josselin & Bachiller (2003); 7: Palla et al. (2000); 8: Cami & Yamamura (2001); 9: Greaves & Holland (1997); 10: Wannier & Sahai (1987); 11: Jaminet et al. (1992).
[c] Doubly peaked.

derived the $CO/^{13}CO$ ratio to be 20 from model analysis on CO ($J = 2-1$) observations and Kahane et al. (1992) obtained the ratio of 32^{+10}_{-7} from observations of CS. Jaminet et al. (1992) have indicated, on the other hand, that the fast wind component has $^{12}C/^{13}C$ of 5 from the wing profile of CO ($J = 3-2$) emissions. Bakker et al. (1997) gave a lower limit of 19 based on the negative detection of circumstellar molecules with ^{13}C. Goto et al. (2002) indicated that the 3.3 μm band profile does not show any spatial variations, suggesting that the extended component of the band emission is the scattered light of the emission from the central region. There is no evidence so far for the spatial variation in the band features within the nebula. Since this object may have a different type of the band carriers, the peak position of the 6.2 μm band (in fact it is located at 6.29 μm) should be discussed separately from other objects. The 8.2 μm band seen in the dark-QCC may correspond to the band at 8.22 μm detected in class *C* objects. It should be noted that the dark-QCC of the natural isotope abundance also has a band at 6.3 μm, shifted to a longer wavelength compared to the filmy-QCC. The 3.3 μm band is seen at the class *B* position and the 11.2 μm is very weak, if present. Differences in the type of the band carriers themselves may account for the observed shift in the 6.2 μm band as suggested by the difference between filmy- and dark-QCC spectra.

As described above, carbon isotope ratios obtained from CO observations of post-AGB stars and PNe are upper limits in most cases or show large scatter because of uncertainties in the observed intensities of faint ^{13}CO emissions (see Josselin & Bachiller 2003) and in the correction for the optical depth effects of ^{12}CO lines. In addition very few objects in the post-AGB phase with the UIR bands have measured $^{12}C/^{13}C$ data, including upper limits. Thus it is difficult at present to directly compare the present results with observations for individual objects. The overall shift pattern of the UIR band peaks is qualitatively in agreement with the isotopic shift pattern except for the 7.7 μm band complex. However, Table 2 does not indicate a quantitatively clear correlation between $^{12}C/^{13}C$ and the peak wavelengths and the suggested ^{13}C abundance in individual objects seems to be slightly too small to account for the observed shifts in terms of the isotopic effects. Observations also indicate that the correlation among the peak wavelengths of the 6–9 μm bands is good, but the peak shifts in the 6–9 μm bands are not tightly correlated with those in the 3.3 and 11.2 μm bands. The UIR band emission is thought to come from the vicinity of the central star, while the CO emission probes the entire region of the circumstellar envelope. Part of the lack of clear correlations and the poor quantitative agreement between the isotope ratio and the peak wavelengths may be attributed to possible spatial variations in the isotope abundance within the object. If the 3.3 and 11.2 μm bands come from regions different (either closer to or farther away from the source) from that of the 6–9 μm bands, the poor correlation of the peak wavelengths among the 3.3, 6–9, and 11.2 μm bands may also be attributed to the spatial variation in the isotope ratio with which each band carrier was formed in the envelope.

Most PAHs have band peaks longer than 6.3 μm for a C=C vibration contrary to the filmy-QCC and it has been suggested that the substitution of a carbon atom by a hetero-atom, such as nitrogen, oxygen, or silicon, will shift the band to shorter wavelengths as observed in class *A* objects (Peeters et al. 2002). Then the observed variations are interpreted in terms of the relative abundance of pure-carbon PAHs and substituted PAHs. The hetero-atom substitution, on the other hand, does not make systematic shifts in other bands. The isotopic substitution of ^{13}C has similar effects on the peak wavelength for the 6.2 μm band but in the opposite direction. In addition it makes systematic shifts in the peak wavelengths of other bands and qualitatively accounts for the observed variations correlated with the 6.2 μm band. The peak wavelength of the C=C stretching vibration band decreases with the size of PAHs, while the increase of the molecular size does not make systematic shifts in the 7.7 μm band (Peeters et al. 2002). Hetero-atom substitutions and size variations are likely to occur in

interstellar medium and the observed variations could be a summation of various processes. The present results indicate that the isotopic effects can contribute to the observed variations for objects with low $^{12}C/^{13}C$ ratios. It should also be emphasized that the peak shifts of the UIR bands are observed mostly in post-AGB stars and PNe, which are the objects where small $^{12}C/^{13}C$ ratios are expected.

It has been suggested that deuterated PAHs (PADs) can be efficiently formed in dense molecular clouds because the large difference in the zero-point energy between H and D containing species leads to preferential formation (fractionation) of deuterated species at low temperatures (e.g. Tielens 1997; Sandford et al. 2000). For the carbon isotope case, the zero-point energy difference is not large and the temperature in the circumstellar envelope is much higher than the zero-point energy. Hence isotopic fractionation should not be significant. Instead a rather large ^{13}C abundance is expected to exist in certain environments and carbonaceous dust that is formed in such environments should show isotopic shifts in its band features. Shifts in the band peaks of PADs from those of PAHs are quite large because of the large mass difference in H and D. Contrary to deuterated species, expected shifts for ^{13}C carbonaceous material are small but should still be in the detectable range as shown by the present results.

5. Summary

We synthesized the QCC, a laboratory analogue of carbonaceous dust, with various ^{13}C fractions and measured the isotopic shifts in the peak wavelengths of the infrared bands. They all shift to longer wavelengths approximately linearly with the ^{13}C fraction. The fact that no separate peaks originating from ^{13}C-QCC appear indicates that the vibration modes of infrared bands associated with carbon atoms in the QCC should not be very localized, but that they stem from rather large structures containing several carbon atoms. The shifts in the 6.2 and 7.8 μm are quite large ($\Delta\lambda > 0.2$ μm per ^{13}C fraction) and that in the 11.2 μm is modest ($\sim$0.16 μm), while the shift in the 3.3 μm band is small (<0.015 μm). The small shift in the 3.3 μm band is in agreement with a simple calculation of benzene molecules and those in the 6.2 and 11.2 μm seem to be larger, also suggesting that a larger number of carbon atoms associated with these bands than benzene. The isotopic shifts obtained in the present experiment are qualitatively in agreement with the shift pattern observed in the peak wavelengths of the UIR bands except for the 7.7 μm band complex. However the observed variations seem to be larger than those inferred from the $^{12}C/^{13}C$ ratio and the quantitative agreement between the carbon isotope ratio and the peak wavelengths is not good for individual objects. This may be attributed partly to large uncertainties in the isotope ratios derived from observations, to possible spatial variations in the isotope abundance in the envelope, and to combinations with other effects, such as heteroatom substitutions. The present results indicate that the isotopic shifts in the peak wavelengths of the UIR bands should be detectable in objects of low $^{12}C/^{13}C$ ratios and part of the observed variations in the band peaks can be attributed to the isotopic effects.

Table A.1. Wavelength of the vibration modes of ^{12}C- and ^{13}C-benzene.

Mode	^{12}C-benzene (μm)	^{13}C-benzene (μm)
λ_{20}	3.245	3.257
λ_{19}	6.812	6.964
λ_{18}	9.524	9.709
λ_{11}	14.90	14.95

Acknowledgements. This work is based in part on observations with ISO, an ESA project with instruments funded by ESA Member States (especially the PI countries: France, Germany, The Netherlands and UK) and with the participation of ISAS and NASA. Part of this work was supported by Grant-in-Aids for Scientific Research from Japan Society for the Promotion of Science.

Appendix A: Calculation of isotopic peak shifts of benzene molecule

In this appendix, we estimate isotopic peak shifts in the vibration modes of a benzene molecule to compare with the isotopic shifts in the corresponding vibration modes of the QCC. Benzene is the simplest PAH and the results should be used as a 0-th order reference in comparison with the isotopic shifts in the QCC.

The GF matrix method is used to calculate isotopic shifts of a benzene molecule (Wilson et al. 1955). The G matrix represents the molecular geometry and the F matrix consists of the force constants. The eigenvalue of the GF matrix is given by $\lambda = 2\pi^2\nu^2$, where ν is the frequency of the vibration mode. In the calculation of the isotopic shift, only the values of the G matrix elements change due to the isotopic substitution and the F matrix elements remain unchanged if all carbon atoms are substituted by ^{13}C. We use the values of the force constants of benzene given by Crawford & Miller (1946, 1949). The vibrational modes of infrared active fundamentals in benzene consist of one A_{2u} (C-H out-of-plane bending) and three E_{1u} (three kinds of in-plane vibrations) modes. The single G matrix element of A_{2u} is written by

$$\mathrm{G}(A_{2u}) = (\mu_H + \mu_C)\,\sigma^2 \tag{A.1}$$

and those of E_{1u} are given by

$$\mathrm{G}(E_{1u}) = \begin{pmatrix} \mu_H + \mu_C & -\frac{\sqrt{3}}{2}\mu_C & \frac{3}{4}\tau\mu_C \\ & \frac{3}{2}\mu_C & -\frac{\sqrt{3}}{4}(2\sigma + 3\tau)\mu_C \\ & & \sigma^2\mu_H + \left(\sigma^2 + \frac{3}{2}\sigma\tau + \frac{9}{8}\tau^2\right)\mu_C \end{pmatrix}, \tag{A.2}$$

where only the upper right elements are shown for the symmetric G matrix. The parameters σ and τ indicate the reciprocals of the C–H and C–C bond lengths, while μ_H and μ_C are the reciprocal masses of H and C, respectively. The bond

angles are all set as 120°. From Eqs. (A.1) and (A.2) and the F matrix we calculate the eigenvalues of the GF matrix and obtain the wavelength ratios of each vibrational mode between ^{12}C-benzene and ^{13}C-benzene. Then the wavelengths of ^{12}C-benzene are scaled to the measured values. The results are listed in Table A.1. Because the wavelength of each mode is different from that in the QCC, we scale the wavelengths of ^{12}C-benzene to the bands measured in the ^{12}C-QCC and estimate the isotopic shifts (Table 1). The λ_{20} mode is scaled to the 3.3 μm band and the λ_{19} mode to the 6.2 μm band. The band at 11.4 μm in the QCC is assigned to a solo or duo C−H out-of-plane bending, which does not have a corresponding mode in benzene. We estimate the isotopic shift by simply scaling the λ_{11} mode to 11.4 μm because it is also a C−H out-of-plane mode of benzene.

References

Allamandola, L. J., Tielens, A. G. G. M., & Barker, J. R. 1985, ApJ, 290, L25

Allamandola, L. J., Hudgins, D. M., & Sandford, S. A. 1999, ApJ, 511, L115

Amari, S., Nittler, L. R., Zinner, E., Lodders, K., & Lews, R. S. 2001, ApJ, 559, 463

Anders, E., & Grevesse, N. 1989, Geochim. Cosmochim. Acta, 53, 197

Arnoult, K. M., Wdowiak, T. J., & Beegle, J. W. 2000, ApJ, 535, 815

Bachiller, R., Forveille, T., Huggins, P. J., & Cox, P. 1997, A&A, 324, 1123

Bakker, E. J., & Lambert, D. L. 1998, ApJ, 508, 387

Bakker, E. J., van Dishoeck, E. F., Waters, L. B. F. M., & Schoenmaker, T. 1997, A&A, 323, 469

Balser, D. S., McMullin, J. P., & Willson, T. L. 2002, ApJ, 572, 326

Beintema, D. A., van den Ancker, M. E., Molster, F. J., et al. 1996, A&A, 315, L369

Bernatowicz, T. J., Amari, S., Zinner, E. K., & Lewis, R. S. 1991, ApJ, 373, L73

Boogert, A. C. A., Ehrenfrend, P., Gerakines, P. A., et al. 2000, A&A, 353, 349

Boulanger, F. 1998, in Star Formation with ISO, ed. J. L. Yun, & R. Liseau, ASP Conf. Ser., 132, 15

Cami, J., & Yamamura, I. 2001, A&A, 367, L1

Cesarsky, D., Lequeux, J., Ryter, C., & Gérin, M. 2000a, A&A, 354, L87

Cesarsky, D., Jones, A. P., Lequeux, J., & Verstraete, L. 2000b, A&A, 358, 708

Clegg, R. E. S., Storey, P. J., Walsh, J. R., & Neale, L. 1997, MNRAS, 284, 348

Crawford, B. L., & Miller, F. A. 1946, J. Chem. Phys., 14, 282

Crawford, B. L., & Miller, F. A. 1949, J. Chem. Phys., 17, 249

de Graauw, T., Haser, L. N., Beintema, D. A., et al. 1996, A&A, 315, L49

Frost, C. A., Cannon, R. C., Lattanzio, J. C., Wood., P. R., & Forestini, M. 1998, A&A, 332, L17

Gilroy, K. K. 1989, ApJ, 347, 835

Goto, M., Kobayashi, N., Terada, H., & Tokunaga, A. T. 2002, ApJ, 572, 276

Greaves, J. S., & Holland, W. S. 1997, A&A, 327, 342

Helou, G., Lu, N., Y., Werner, M. W., et al. 2000, ApJ, 532, L21

Henkel, C., Walmsley, C. M., & Wilson, T. L. 1980, A&A, 82, 41

Holmid, L. 2000, A&A, 358, 276

Hony, S., Van Kerckhoven, C., Peeters, E., et al. 2001, A&A, 370, 1030

Jaminet, P. A., Danchi, W. C., Sandell, G., & Sutton, E. C. 1992, A&A, 400, 535

Joblin, C., Boissel, P., Léger, A., d'Hendecourt, L., & Défourneau, D. 1995, A&A, 299, 835

Jones, A. P., & d'Hendecourt, L. 2000, A&A, 355, 1191

Josselin, E., & Bachiller, R. 2003, A&A, 397, 659

Josselin, E., & Lébre, A. 2001, A&A, 367, 826

Kahane, C., Cernicharo, J., Gómez-González, J., & Guélin, M. 1992, A&A, 256, 235

Kahanpää, J., Mattila, K., Lehtinen, K., Leinert, C., & Lemke, D. 2003, A&A, 405, 999

Kessler, M. F., Steinz, J. A., Anderegg, M. E., et al. 1996, A&A, 315, L27

Kerr, T. H., Hurst, M. E., Miles, J. R., & Sarre, P. J. 1999, MNRAS, 303, 446

Lambert, D. L., Gustafsson, B., Eriksson, K., & Hinkle, K. H. 1986, ApJS, 62, 373

Leech, K., de Graauw, T., van den Ancker., et al. 2002, The ISO Handbook, vol VI: SWS–The Short Wavelength Spectrometer, ver2.0

Léger, A., & Puget, J. L. 1984, A&A, 137, L5

Likkel, L., Forveille, T., Omont, A., & Morris, M. 1988, A&A, 198, L1

Lu, N., Helou, G., Werner, M. W., et al. 2003, ApJ, 588, 199

Mattila, K., Lemke, D., Haikala, L. K., et al. 1996, A&A, 315, L353

Mamon, G. A., Glassgold, A. E., & Huggings, P. J. 1988, ApJ, 328, 797

Mattila, K., Lehtinen, K., & Lemke, D. 1999, A&A, 342, 643

Men'shchikov, A. B., Schertl, D., Tuthill, P. G., Weigelt, G., & Yungelson, L. R. 2002, A&A, 393, 867

Molster, F. J., van den Ancker, M. E., Tielens, A. G. G. M., et al. 1996, A&A, 315, L373

Moutou, C., Verstraete, L., Léger, A., Sellgren, K., & Schmidt, W. 2000, A&A, 354, L17

Nagata, T., Tokunaga, A. T., Sellgren, K., et al. 1988, ApJ, 326, 157

Nollett, K. M., Busso, M., & Wasserburg, G. J. 2003, ApJ, 582, 1036

Ohnaka, K., & Tsuji, T. 1996, A&A, 310, 933

Onaka, T., Yamamura, I., Tanabé, T., Roellig, T. L., & Yuen, L. 1996, PASJ, 48, L59

Palla, F., Bachiller, R., Stanghellini, L., Tosi, M., & Galli, D. 2000, A&A, 355, 69

Papoular, R., Conard, J., Giuliano, M., Kister, J., & Mille, G. 1989, A&A, 217, 204

Pech, C., Joblin, C., & Boissel, P. 2002, A&A, 388, 639

Peeters, E., Hony, S., Van Kerckhoven, C., et al. 2002, A&A, 390, 1089

Reach, W. T., Boulanger, F., Contursi, A., & Lequeux, J. 2000, A&A, 361, 895

Roche, P. F., Aitken, D. K., & Smith, C. H. 1991, MNRAS, 252, 282

Sakata, A., Wada, S., Tanabe, T., & Onaka, T. 1984, ApJ, 287, L51

Sakata, A., Wada, S., Onaka, T., & Tokunaga, A. T. 1987, ApJ, 320, L63

Sakata, A., Wada, S., Onaka, T., & Tokunaga, A. T. 1990, ApJ, 353, 543

Sakata, A., Wada, S., Narisawa, T., et al. 1992, ApJ, 393, L83

Sandford, S. A., Burnstein, M. P., Allamandola, L. J., Gillette, J. S., & Zare, R. N. 2000, ApJ, 538, 691

Savage, C., Apponi, A. J., Ziurys, L. M., & Wyckoff, S. 2002, ApJ, 578, 211

Schöier, F. L., & Olofsson, H. 2000, A&A, 359, 586

Song, I.-O., McCombie, J., Kerr, T. H., Couch, P. A., & Sarre, P. J. 2003, poster presentation at Astrophysics of Dust 2003, Colorado

Tanaka, M., Matsumoto, T., Murakami, H., et al. 1996, PASJ, 48, L53
Tielens, A. G. G. M. 1997, in Astrophysical Implications of the Laboratory Study of Presolar Materials, ed. T. J. Bernatowicz, & E. Zinner (Woodbury: AIP), AIP Conf. Proc. 402, 523
Tokunaga, A. T. 1997, in Diffuse Infrared Radiation and the IRTS, ed. H. Okuda, T. Matsumoto, & T. L. Roellig (San Franscisco: ASP), ASP Conf Ser. 124, 149
Tokunaga, A. T., Nagata, T., Sellgren, K., et al. 1988, ApJ, 328, 709
Tokunaga, A. T., Sellgren, K., Smith, R. G., et al. 1991, ApJ, 380, 452
Uchida, K. I., Sellgren, K., & Werner, M. W. 1998, ApJ, 493, L109
Uchida, K. I., Sellgren, K., Werner, M. W., & Houdashelt, M. L. 2000, ApJ, 530, 817
van Diedenhoven, B., Peeters, E., Van Kerckhoven, C., et al. 2003, in preparation
Verstraete, L., Puget, J. L., Falgarone, E., et al. 1996, A&A, 315, L337
Verstraete, L., Pech, C., Moutou, C., et al. 2001, A&A, 372, 981
Wada, S., Kaito, C., Kimura, S., Ono, H., & Tokunaga, A. T. 1999, A&A, 345, 259
Wannier, P. G., & Sahai, R. 1987, ApJ, 319, 367
Wasserburg, G. J., Boothroyd, A. I., & Sackmann, I.-J. 1995, ApJ, 447, L37
Waters, L. B. F. M., Cami, J., de Jong, T., et al. 1998, Nature, 391, 868
Wilson, T. L. 1999, Rep. Prog. Phys., 62, 143
Wilson, E. B. Jr., Decius, J. C., & Cross, P. C. 1955, Molecular Vibrations, The Theory of Infrared and Raman Vibrational Spectra (New York: McGraw-Hill Book Company, Inc.)